Electrochimica Acta 438 (2023) 141461

Contents lists available at ScienceDirect

Electrochimica Acta

journal homepage: www.journals.elsevier.com/electrochimica-acta

A fractional-order model of lithium-ion battery considering polarization in electrolyte and thermal effect

Guorong Zhu [a], Chun Kong [a], Jing V. Wang [a,*], Jianqiang Kang [b,c], Geng Yang [d], Qian Wang [a]

[a] School of Automation, Wuhan University of Technology, Wuhan 430070, PR China
[b] Hubei Key Laboratory of Advanced Technology for Automotive Components, Wuhan University of Technology, Wuhan 430070, PR China
[c] Hubei Collaborative Innovation Center for Automotive Components Technology, Wuhan 430070, PR China
[d] Department of Automation, Tsinghua University, Beijing 100084, PR China

ARTICLE INFO

Keywords:
Lithium-ion battery
Fractional-order model
Electrolyte polarization
Thermal effect

ABSTRACT

With the growing demand of safety and accurate control for electric vehicles, it is urgent to develop a physics-based electrochemical model of lithium-ion battery with simple calculation and high accuracy over wide temperature range for application in battery management system (BMS). However, traditional electrochemical models are too complex to be applied in real usage, and most of them fail to capture thermal characteristics of the cell. Therefore, a fractional-order model of lithium-ion battery considering polarization in electrolyte and thermal effect (FOMeT) is proposed in this paper. The fractional-order model (FOM) is improved by considering the polarization in electrolyte. The particle thermal model is proposed to describe the heat generation and absorption of the cell. Finally, the FOM considering electrolyte polarization and the particle thermal model are combined to form FOMeT by coupling the cell temperature and dynamics of lithium-ion. The results show that the proposed model performs high voltage accuracy and temperature accuracy over wide temperature range (273.15K~318.15K) and wide current load range (0.5C~2C).

1. Introduction

In response to the energy crisis and environmental pollution, lithium-ion batteries are gradually being widely used in electric vehicles, ships, and other high-power and large-scale energy storage equipment [1]. To ensure the efficient and reliable operation of power batteries, it is necessary to establish an utilitarian battery model and achieve accurate estimation of basic state quantities such as cell voltage and state of charge (SOC) [2]. Equivalent circuit models (ECMs) have been widely used in lithium-ion battery modeling because of its simple structure and parameters that are easy to identify [3]. However, there are some problems in equivalent circuit models, such as bad generalization ability, low prediction accuracy, and weak parameter interpretability [4]. Such weaknesses limit the further application of equivalent circuit models in future BMS. To deal with the shortcomings of equivalent circuit models, Newman et al. [5] proposed a pseudo-two-dimensional (P2D) electrochemical model in 1993. Compared with equivalent circuit models, the P2D model can describe internal dynamics of the cell, explain the physical mechanism, and have more advantages in cell voltage prediction and SOC estimation [6].

Due to the existence of a series of strongly coupled nonlinear partial differential equations in the full-order P2D model, its computational complexity is relatively high [7]. It is hard to apply P2D model in real-time BMS, so it is necessary to simplify the full-order P2D model to reduce its computational complexity. HAN et al. [8] proposed an effective method to solve nonlinear partial differential equations in full-order P2D lithium-ion battery model. Their simulation results were able to accurately match the results of full-order P2D model in COMSOL Multiphysics, but the calculation speed is still lower than that of reduced order P2D models. In order to further simplify the P2D model and speed up the calculation, the single particle (SP) model was proposed [9]. The SP model ignores the electrolyte polarization inside the cell, and the electrode is equivalent to a single particle, so the governing partial differential equations can be simplified into a set of algebraic equations [10]. Guo et al. [11] proposed a fractional-order model (FOM) based on the SP model, which simplified solid phase diffusion with Padé approximation. The FOM achieves the same voltage prediction accuracy

* Corresponding author.
E-mail address: jingvwang@whut.edu.cn (J.V. Wang).

https://doi.org/10.1016/j.electacta.2022.141461
Received 21 July 2022; Received in revised form 27 October 2022; Accepted 30 October 2022
Available online 31 October 2022

as the SP model, but greatly saves computational time. Tian et al. [12] proposed a novel online method to identify the parameters and order of FOM, compared with the fixed-order method under different operation conditions, their method has achieved better accuracy and robustness of identified model parameters. Since both the SP model and FOM do not consider the distribution of electrolyte potential of lithium-ion battery, the voltage prediction error of the SP model is relatively large under high rate charge and discharge [13,14]. Moura et al. [15] proposed a single particle model with electrolyte dynamics (SPMe), they designed a electrolyte observer to describe the electrolyte polarization of lithium-ion battery. The experimental results show that SPMe still has high accuracy under high rate charge and discharge.

Temperature has a great influence on electrochemical reaction of lithium-ion battery and the diffusion of lithium-ion in the solid and electrolyte phase [16]. To improve the applicability of the electrochemical model over a wide temperature range, it is necessary to study the electrochemical model considering wide range thermal dynamics. Li et al. [17] established a high-accuracy simplified electrochemical model and identified its parameters over a wide temperature range. The results show that the simplified electrochemical model considering thermal dynamics can predict the cell voltage and temperature with high accuracy. Ma et al. [18] proposed a one-dimensional electrochemical model coupled thermal for SOC estimation, and the maximum SOC error is about 2%. However, their proposed model, whose parameters are difficult to obtain, is still complicated. Although many physics-based electrochemical models have been studied, most of them are too complicated to be applied in BMS and fail to capture the thermal characteristics of lithium-ion battery, which limits the model accuracy over wide temperature range. It is of great significance to apply a physics-based electrochemical model with simple calculation and high accuracy over wide temperature range in BMS.

Therefore, a fractional-order model of lithium-ion battery considering polarization in electrolyte and thermal effect (FOMeT) is proposed in this paper. Three contributions are made in this paper:

1 In order to improve the voltage accuracy of FOM at high current rate, the FOM is developed by considering polarization in electrolyte. The lithium-ion diffusion in electrolyte is simplified by the polynomial approximation method to reduce the computation complexity.
2 The particle thermal model is proposed to simplify the 3D thermal model, so that it can be integrated into the FOM considering electrolyte polarization.
3 According to the above innovations, a coupling model of the fractional-order model considering electrolyte polarization and the particle thermal model is proposed. The proposed model, considers polarization in electrolyte and thermal effect, can capture lithium-ion dynamics at different temperatures.

The structure of this study is organized as follows. In Section 2, the mechanism of the simplified electrochemical model and the particle thermal model is clarified, and the coupling of the simplified electrochemical model and the particle thermal model is established. In Section 3, the identification and verification of important parameters in FOMeT are completed, and the simulation results of FOMeT are compared with the P2D thermal model. In Section 4, the conclusion is made.

2. Model establishment and mechanism analysis

2.1. Fractional-order model considering polarization in electrolyte

2.1.1. Solid phase diffusion simplified by PADÉ approximation

The charge and discharge of lithium-ion battery is the process of intercalation and deintercalation of lithium-ion in electrode particles. Assuming that the applied current I flowing through the cell is uniformly distributed [19], the pore wall flux of lithium-ion at the positive and negative electrodes of the cell can be expressed as [6]

$$J_i = \frac{IR_{s,i}}{3\varepsilon_{s,i}FAL_i}, i = n, p \tag{1}$$

where R_s is the particle radius of the electrode particles, ε_s is the volume fraction of solid phase, F is Faraday constant, A is the surface area of electrodes, L is the length of electrodes, n, p represent the negative and positive electrodes of the cell, respectively. The inflow current of lithium-ion into the electrode particles is defined as positive and the current of lithium-ion flowing out of the electrode particles is defined as negative.

The lithium-ion capacity of the electrode is related to the volume of the electrode and the maximum lithium-ion concentration of the electrode material, the lithium-ion capacity of electrode is defined as [6]

$$Q_i = A \cdot L_i \cdot \varepsilon_{s,i} \cdot F \cdot c_{s,i}^{\max}, i = n, p \tag{2}$$

where Q_n, Q_p represent negative and positive electrodes capacity, respectively. $c_{s,n}^{\max}$, $c_{s,p}^{\max}$ represent the maximum lithium-ion concentration of the negative and positive electrodes, respectively.

The lithium-ion concentration stoichiometry of the positive and negative electrodes is defined as the ratio of the solid phase lithium-ion concentration to the solid phase maximum lithium-ion concentration, then the initial lithium-ion concentration stoichiometry and the average lithium-ion concentration stoichiometry of the positive and negative electrodes can be expressed as [6]

$$x_0 = \frac{c_{s,n}^0}{c_{s,n}^{\max}}, y_0 = \frac{c_{s,p}^0}{c_{s,p}^{\max}}, x_{mean} = \frac{c_{s,n}^{mean}}{c_{s,n}^{\max}}, y_{mean} = \frac{c_{s,p}^{mean}}{c_{s,p}^{\max}} \tag{3}$$

The average lithium-ion concentration stoichiometry of the positive and negative electrodes can be calculated by the initial lithium-ion concentration stoichiometry and coulomb counting.

$$x_{mean} = x_0 + \frac{1}{Q_n}\int_0^{t_k} I(t)dt \tag{4}$$

$$y_{mean} = y_0 - \frac{1}{Q_p}\int_0^{t_k} I(t)dt \tag{5}$$

The negative electrode is taken as an example for deriving simplified solid phase diffusion. The diffusion of lithium-ion in solid phase is governed by Fick's second law [20].

$$\frac{\partial c_{s,n}(r,t)}{\partial t} = \frac{D_{s,n}}{r^2}\frac{\partial}{\partial r}\left(r^2\frac{\partial c_{s,n}(r,t)}{\partial r}\right), 0 \le r \le R_{s,n} \tag{6}$$

where $c_{s,n}(r,t)$ is the solid phase lithium-ion concentration of negative electrode, $D_{s,n}$ is the negative solid phase diffusion coefficient, $R_{s,n}$ is the negative particle radius. The boundary conditions of Eq. (6) are

$$D_{s,n}\frac{\partial c_{s,n}(0,t)}{\partial r} = 0, \quad D_{s,n}\frac{\partial c_{s,n}(R_s,t)}{\partial r} = j(t) \tag{7}$$

By Laplace transformation of Eq. (6) and combining its boundary conditions Eq. (7), the relationship between the change of the negative electrode surface lithium-ion concentration relative to the negative electrode initial lithium-ion concentration $\tilde{c}_{s,n}^{surf}$ and the applied current I can be obtained [21,22], as shown in Eq. (8).

$$\frac{\tilde{c}_{s,n}^{surf}}{I} = \frac{R_{s,n}^2}{3\varepsilon_{s,n}FAL_nD_{s,n}}\left[\frac{1}{\sqrt{\frac{R_{s,n}^2}{D_{s,n}}s}\coth\left(\sqrt{\frac{R_{s,n}^2}{D_{s,n}}s}\right) - 1}\right] \tag{8}$$

where $\tilde{c}_{s,n}^{surf} = c_{s,n}^{surf} - c_s^0$ is the difference between the lithium-ion concentration on the negative electrode surface and the initial

negative electrode lithium-ion concentration. The time constant τ_n is defined as

$$\tau_n = \frac{R_{s,n}^2}{D_{s,n}} \tag{9}$$

Since there is a pole at $s = 0$ in Eq. (8), the system is unstable. To make a stable transfer function, define the solid surface lithium-ion concentration change after removing the integrator pole as $\Delta\widetilde{c}_{s,n}^{surf} = \widetilde{c}_{s,n}^{surf} - c_{s,n}^{mean}$. The relationship between $\Delta\widetilde{c}_{s,n}^{surf}$ and the applied current I can be expressed as

$$\frac{\Delta\widetilde{c}_{s,n}^{surf}}{I} = \frac{\tau_n}{3\varepsilon_{s,n}FAL_n}\left[\frac{1}{\sqrt{\tau_n s}\coth\left(\sqrt{\tau_n s}\right) - 1} - \frac{3}{\tau_n s}\right] \tag{10}$$

For simplifying the solid phase diffusion, the Padé approximation is applied to describe the solid phase diffusion, as shown in Eq. (11).

$$\frac{\Delta\widetilde{c}_{s,n}^{surf}}{I} = \frac{\tau_n}{3\varepsilon_{s,n}FAL_n}\left[\frac{a}{1 + b\sqrt{\tau_n s}}\right] \tag{11}$$

The derivation of the solid phase diffusion of positive electrode is similar to that of negative electrode, the relationship between $\Delta\widetilde{c}_{s,p}^{surf}$ and the applied current I can be expressed as

$$\frac{\Delta\widetilde{c}_{s,p}^{surf}}{I} = \frac{\tau_p}{3\varepsilon_{s,p}FAL_p}\left[\frac{a}{1 + b\sqrt{\tau_p s}}\right] \tag{12}$$

Then, the lithium-ion concentration stoichiometry on the surface of positive and negative electrode particles can be expressed as

$$x_{surf} = x_{mean} + \frac{\Delta\widetilde{c}_{s,n}^{surf}}{c_{s,n}^{\max}} \tag{13}$$

$$y_{surf} = y_{mean} - \frac{\Delta\widetilde{c}_{s,p}^{surf}}{c_{s,p}^{\max}} \tag{14}$$

The open circuit potential of the electrode is determined by the lithium-ion concentration stoichiometry on the surface of positive and negative particles, and the difference between the open circuit potential of positive and negative electrodes is the open circuit voltage of the cell E_{batt}.

$$E_{batt} = U_p\left(y_{surf}\right) - U_n\left(x_{surf}\right) \tag{15}$$

2.1.2. Electrolyte phase diffusion simplification

The electrolyte diffusion overpotential is caused by the uneven distribution of lithium-ion concentration in the electrode thickness direction due to the diffusion of lithium-ion in the electrolyte solution [23]. For simplification, the electrolyte phase volume fractions of the positive electrode, separator, and negative electrode of the cell are assumed to be equal [24]. The change of the electrolyte phase lithium-ion concentration at the terminal of the positive and negative electrodes can be simplified as [17]

$$\begin{cases} \dfrac{d}{dt}c_{e,n}^{diff} = \dfrac{D_e\varepsilon_e^{brugg}}{P}c_{e,n}^{diff} + \dfrac{1 - t_+}{FAPQ_1}I \\ \dfrac{d}{dt}c_{e,p}^{diff} = \dfrac{D_e\varepsilon_e^{brugg}}{P}c_{e,p}^{diff} + \dfrac{1 - t_+}{FAPQ_2}I \end{cases} \tag{16}$$

where $c_{e,i}^{diff} = c_{e,i} - c_e^0, \quad i = n,p$ is the difference between the electrolyte phase lithium-ion concentration at electrode terminal $c_{e,i}$ and the initial electrolyte phase lithium-ion concentration c_e^0. D_e is the electrolyte phase diffusion coefficient, ε_e is the volume fraction of electrolyte phase, *brugg* is the Bruggman coefficient, and t_+ is the particle migration number. P, Q_1, Q_2, can be calculated as Eq. (17).

$$\begin{cases} P = -\varepsilon_e\left(\dfrac{1}{3}L_n^2 + L_n x_{equ} + \dfrac{1}{2}x_{equ}^2\right) \\ Q_1 = -\dfrac{2}{L_n + 2x_{equ}} \\ Q_2 = -\dfrac{2}{L_p + 2\left(L_{sep} - x_{equ}\right)} \\ x_{equ} = \dfrac{-2L_n^2 + 3L_{sep}^2 + 2L_p^2 + 6L_{sep}L_p}{6\left(L_n + L_{sep} + L_p\right)} \end{cases} \tag{17}$$

where L_p is the thickness of positive electrode, L_{sep} is the thickness of separator, L_n is the thickness of negative electrode.

The electrolyte phase lithium-ion concentration at the terminal of the positive and negative electrodes directly affects the electrolyte diffusion overpotential, the overpotential can be calculated from the electrolyte phase lithium-ion concentration at the terminal of the two electrodes [17], as shown in Eq. (18).

$$\eta_{c_e}(t) = (1 - t_+)\frac{2R_gT}{F}\ln\frac{c_{e,p}}{c_{e,n}} \tag{18}$$

where η_{c_e} is the electrolyte diffusion overpotential, R_g is the ideal gas constant, T is the cell temperature.

2.1.3. Activation overpotential

The lithium-ion pore wall flux on the surface of electrodes also characterizes the speed of the electrochemical reaction. The Bulter-Volmer (B-V) equation can be used to describe the chemical reaction of lithium-ion intercalation and deintercalation [25].

$$J = \frac{i_0}{F}\left[\exp\left(\frac{F}{2R_gT}\eta_{ct}\right) - \exp\left(-\frac{F}{2R_gT}\eta_{ct}\right)\right] \tag{19}$$

$$i_0 = k_i\left(c_{e,i}\right)^{0.5}\left(c_{s,i}^{\max} - c_{s,i}^{surf}\right)^{0.5}\left(c_{s,i}^{surf}\right)^{0.5} i = n,p \tag{20}$$

where η_{ct} is the activation overpotential, k is the electrochemical reaction coefficient, i_0 is the exchange current density of the electrochemical reaction. Therefore, the activation overpotential can be calculated by Eq. (21).

$$\eta_{ct} = \frac{2R_gT}{F}\left[\ln\left(\sqrt{m_p^2 + 1} + m_p\right) - \ln\left(\sqrt{m_n^2 + 1} + m_n\right)\right] \tag{21}$$

$$m_i = 0.5J_i\Big/\left[k_i\left(c_{e,i}\right)^{0.5}\left(c_{s,i}^{\max} - c_{s,i}^{surf}\right)^{0.5}\left(c_{s,i}^{surf}\right)^{0.5}\right] i = n,p \tag{22}$$

2.1.4. Ohmic overpotential

Ohmic resistance is a lumped parameter describing the high-frequency dynamic response inside the cell, which is mainly composed of solid and electrolyte phase charge transfer resistance, solid electrolyte interphase (SEI) layer resistance, and contact resistance.

$$R_{ohm} = R_{s,ohm} + R_{e,ohm} + R_{SEI} + R_{cont} \tag{23}$$

where R_{SEI} is an equivalent resistance of SEI layer, R_{cont} is the contact resistance of the cell. $R_{s,ohm}$and $R_{e,ohm}$ are charge transfer resistance of solid phase and electrolyte phase, respectively, which can be expressed as [17]

$$R_{s,ohm} = \frac{L_n}{k_{s,n}A} + \frac{L_p}{k_{s,p}A} \tag{24}$$

$$R_{e,ohm} = \frac{L_n}{2k_{e,n}^{eff}A} + \frac{L_{sep}}{k_{e,sep}^{eff}} + \frac{L_p}{2k_{e,p}^{eff}A} \tag{25}$$

where $k_{s,p}$ and $k_{s,n}$ are the solid phase conductivity of the positive and negative electrodes, respectively. $k_{e,p}^{eff}$, $k_{e,sep}^{eff}$, and $k_{e,n}^{eff}$ are the effective

electrolyte phase conductivity of the positive electrode, separator, and negative electrode, respectively. The ohmic overpotential of the cell can be expressed as

$$\eta_{ohm} = R_{ohm} I \tag{26}$$

The terminal voltage of the cell can be expressed as

$$V_{cell} = E_{batt} + \eta_{c_e} + \eta_{ct} + \eta_{ohm} \tag{27}$$

2.2. Particle thermal model

2.2.1. Cell heat generation

With the cell charging and discharging, the mutual conversion of electrical energy and chemical energy occurs inside the cell, and it is also accompanied by heat generation and absorption. According to Bernardi simplified temperature field theory [26], the internal heat generated in the cell during charging and discharging can be divided into reversible heat and irreversible heat

$$Q_{gen} = \underbrace{I(V_{cell} - E_{batt})}_{Q_{ir}} + \underbrace{\left(\frac{\partial U_p}{\partial T}\Big|_{y_{mean}} - \frac{\partial U_n}{\partial T}\Big|_{x_{mean}}\right) IT}_{Q_r} \tag{28}$$

where Q_{gen} is the total heat generation of the cell, Q_{ir} and Q_r are the irreversible heat generation and reversible heat generation of the cell, respectively. $\frac{\partial U_p}{\partial T}|_{y_{mean}}$ and $\frac{\partial U_n}{\partial T}|_{x_{mean}}$ are the positive and negative entropy heat coefficients, respectively.

2.2.2. Cell temperature

In order to simplify the battery thermal model, the influence of the cell 3-dimensional temperature gradient is ignored. The average cell temperature is regarded as the cell temperature [27], the cell is regarded as a particle heat source, then the cell temperature satisfies the following heat balance equation [16]

$$mC_p \frac{dT}{dt} = Q_{gen} - \lambda(T - T_{amb}). \tag{29}$$

where m is the mass of the cell, C_p is the specific heat capacity of the cell, λ is heat dissipation coefficient of the cell, T_{amb} is ambient temperature.

2.3. Fractional-order model considering polarization in electrolyte and thermal effect

2.3.1. Temperature dependent parameters of FOMe

The solid phase diffusion coefficient, electrolyte phase diffusion coefficient, electrochemical reaction coefficient, and ohmic resistance of fractional-order model considering electrolyte polarization (FOMe) are all affected by temperature [28], and these parameters conform to Arrhenius equation [16]

$$X = X_{ref} \exp\left(\frac{E_a}{R_g}\left(\frac{1}{T_{ref}} - \frac{1}{T}\right)\right) \tag{30}$$

where X is the parameter that conforms to Arrhenius equation, X_{ref} is the value of the parameter at the reference temperature, E_a is the activation energy of the parameter, T_{ref} is the reference temperature.

2.3.2. Coupling of FOMe and particle thermal model

Temperature dependent parameters in FOMe are affected by cell temperature. The change of these parameters also affects FOMe's output, then affects the heat generation and temperature of the cell. The coupling relationship between FOMe and particle thermal model is shown in Fig. 1.

The solid and electrolyte phase diffusion coefficient, electrochemical reaction coefficient, ohmic resistance, and average cell temperature in FOMeT are updated iteratively with the cell charging and discharging.

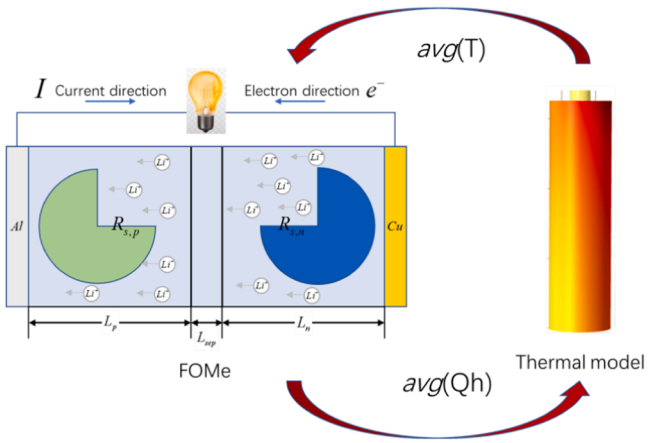

Fig. 1. The coupling relationship between FOMe and thermal model.

Table 1
Activation energy corresponding to parameters affected by temperature [29,30].

Activation energy	Positive	negative
Solid phase diffusion EaD (J/mol)	20,000	68,025.7
Electrochemical reaction EaK (J/mol)	30,000	30,000

Table 1 lists the activation energy corresponding to the parameters affected by temperature.

The electrolyte phase diffusion coefficient is related to both temperature and electrolyte phase lithium-ion concentration. According to Ref. [31], the relationship among temperature, electrolyte phase lithium-ion concentration, and electrolyte phase diffusion coefficient is shown as Eq. (31).

$$D_e = 1 \times 10^{-8.43 - \left(\frac{54}{T - 5\times10^{-3}\times c_e - 229}\right) - 2.2\times10^{-4}\times c_e} \tag{31}$$

The ohmic resistance is a high-frequency lumped parameter, and the value of the ohmic resistance will be obtained through hybrid pulse power characteristic (HPPC) simulation experiments at different temperature in the following section.

3. Simulation and verification

3.1. Parameter identification and validation

3.1.1. Identification of the Padé approximation function coefficients

The Padé approximation function is used to describe the relationship between the solid phase electrode surface lithium-ion concentration change $\Delta\tilde{c}_{s,i}^{surf}$ and the applied current I. The Padé approximation coefficients are found by particle swarm optimization (PSO) [32], which minimizes the root mean square error (RMSE) between the approximate solution of FOMeT and the theoretical exact solution. The objective function is defined as the RMSE between the model output value $\Delta\tilde{c}_{s,n}^{surf}$ and the true value $\Delta\hat{c}_{s,n}^{surf}$, as shown in Eq. (32).

$$L = \sqrt{\frac{1}{t_{all}}\int_0^{t_{all}} \left(\Delta\hat{c}_{s,n}^{surf}(t) - \Delta\tilde{c}_{s,n}^{surf}(t)\right)^2 dt} \tag{32}$$

where t_{all} is the total operation time. The variation of solid phase electrode surface lithium-ion concentration calculated by the full-order P2D model is taken as the true value. The optimal Padé approximation coefficients optimized by PSO are $a = 0.24419$ and $b = 0.14257$, respec-

tively. Therefore, the relationship between $\Delta\widetilde{c}_{s,n}^{surf}$ and the applied current I simplified by Padé approximation can be expressed as

$$\frac{\Delta\widetilde{c}_{s,n}^{surf}}{I} = \frac{\tau_n}{3\varepsilon_{s,n}FAL_n}\left[\frac{0.24419}{1+0.14257\sqrt{\tau_n}s}\right] \tag{33}$$

The LMO battery is used for simulation verification, and the simulation parameters are shown in Table 2.

The LMO battery simulation runs under 2000s discharging, 300 s resting, 2000s charging, and 3700 s resting at 1C rate. The solid phase lithium-ion concentration stoichiometry on the surface of positive and negative electrodes of FOMeT and the solid phase lithium-ion concentration stoichiometry on the surface of positive and negative electrodes of P2D model are compared, as shown in Fig. 2.

In Fig. 2, the outputs of P2D model are taken as actual cell outputs, x_{surf} and y_{surf} of FOMeT fit those of P2D model well, and the RMSE of y_{surf} and x_{surf} between FOMeT and P2D model are 0.0025 and 0.0023, respectively. The mean absolute percentage error (MAPE) of y_{surf} and x_{surf} of FOMeT compared to those of P2D model are 0.91% and 0.45%, respectively. The results show that the Padé approximation can accurately describe the relationship between the solid phase electrode surface lithium-ion concentration change $\Delta\widetilde{c}_{s,i}^{surf}$ and the applied current I.

3.1.2. Identification of ohmic resistance

The ohmic resistance in the cell is a lumped parameter, which includes solid and electrolyte conductivity, SEI film resistance, and contact resistance. The ohmic resistance will also change with temperature. A P2D model is built to identify the ohmic resistance at different temperature by HPPC, and the ohmic resistance changes with temperature as shown in Fig. 3. The ohmic resistance of the cell decreases approximately linearly with the increase of temperature.

3.1.3. Heat dissipation coefficient identification

The objective function is defined as the RMSE between the FOMeT average temperature and the actual cell temperature, as shown in Eq. (34).

$$L = \sqrt{\frac{1}{t_{all}}\int_0^{t_{all}}\left(\widehat{T}(t)-T(t)\right)^2 dt} \tag{34}$$

where $\widehat{T}(t)$ is the output temperature of FOMeT, $T(t)$ is the cell average temperature which is replaced by the average temperature of P2D thermal model. The PSO is also used to find the heat dissipation coefficient that minimizes the error between the output temperature of FOMeT and the average temperature of P2D thermal model. The mass and the specific heat capacity in the simulation are set as 0.80645kg and 1105.9J/(kg*K), respectively. The identified equivalent heat dissipation coefficient λ is 0.7489 W/K. The ambient and initial cell temperature are set as 273.15 K and 298.15 K, respectively. The cell is in a resting state to simulate the heat dissipation. The temperature comparison between FOMeT and P2D thermal model is shown in Fig. 4.

In Fig. 4, the temperature of FOMeT is extremely close to the temperature of P2D thermal model, where the RMSE is about 0.0035 K. The result shows that the identified heat dissipation coefficient λ can effectively reflect the cell heat dissipation.

Table 2
The parameters of LMO battery [33].

Parameter	Negative electrode	Separator	Positive electrode
L(m)	100e−6	52e−6	183e−6
R_s(m)	12.5e−6		8e−6
ε_s	0.471		0.297
ε_e	0.4	0.4	0.4
$c_{s,max}$(mol/m^3)	26,390		22,860
$c_{s,0}$(mol/m^3)	14,870		3900
D_s(m^2/s)	2.6188e−14		1e−14
i_0(A/m^2)	17.71		16.74
$T_{ref}(K)$	298.15		
$c_{e,0}$(mol/m^3)	2000		
D_e(m^2/s)	$D_e = 1\times10^{-8.43-\left(\frac{54}{T-5\times10^{-3}\times c_e-229}\right)}-2.2\times10^{-4}\times c_e$		
t_+	0.363		
F(C/mol)	96,485.33		
R_g(J/mol/K)	8.314		
A(m^2)	1		
$U_p(y)$	$U_p(y) = 4.19829 + 0.0565661\tanh(-14.5546y+8.60942) - 0.0275479\left[\frac{1}{(0.998432-y)^{0.492465}}-1.90111\right] - 0.157123\exp(-0.04738y^8) + 0.810239\exp[-40(y-0.133875)]$		
$U_n(x)$	$U_n(x) = -0.16 + 1.32\exp(-3.0x) + 10.0\exp(-2000.0x)$		

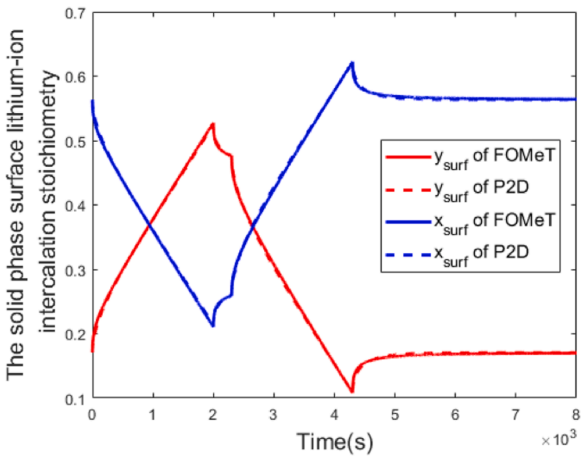

Fig. 2. The solid phase surface lithium-ion intercalation stoichiometry of FOMeT and P2D model.

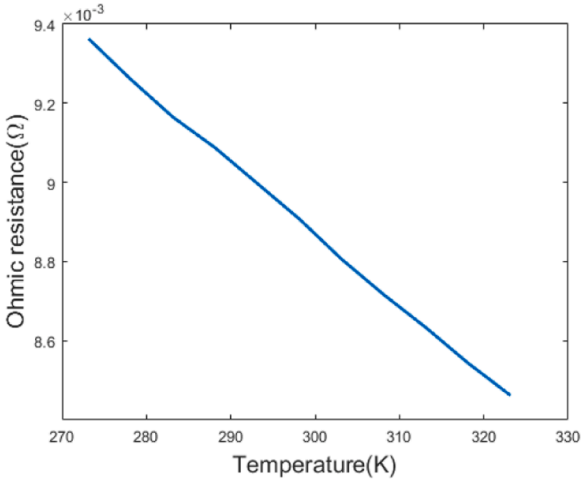

Fig. 3. Ohmic resistance changes with temperature.

3.2. Model simulation and verification

A 17.5Ah LMO cell is used for simulation, and its parameters are shown in Table 2. FOMeT and P2D thermal model simulate discharging for 2000s, resting for 300 s, charging for 2000s, and resting for 3700 s at 298.15 K ambient temperature at 1C rate. The temperature and voltage of FOMeT and P2D thermal model are shown in Fig. 5.

Fig. 5(a) shows the temperature change of FOMeT and P2D thermal model under galvanostatic charge-discharge. The FOMeT temperature curve closely matches that of P2D thermal model. The RMSE of FOMeT

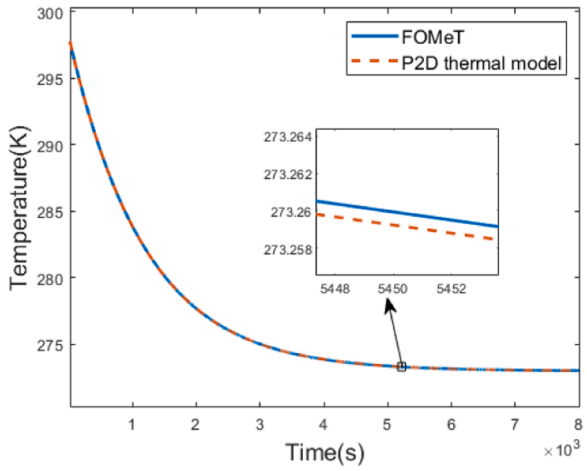

Fig. 4. Resting temperature comparison between FOMeT and P2D thermal model.

temperature compared to that of P2D thermal model is 0.009 K. The maximum temperature rises of FOMeT and P2D thermal model are 4.875 K and 4.885 K, respectively. The voltage of FOM is also added for comparison in Fig. 5(b). The temperature rise of the cell is small at the initial stage of discharge. Such small change has little effect on FOMeT temperature dependent parameters. Therefore, the voltage error between FOMeT and FOM is small at the initial stage of discharge. However, as cell temperature rises, the change of temperature dependent parameters in FOMeT becomes large. The voltage error between FOMeT and FOM then becomes large. The voltage RMSE of FOMeT and FOM compared with the P2D thermal model are 14.4 mV and 16.4 mV, respectively. The voltage MAPE of FOMeT and FOM compared with the P2D thermal model are 0.31% and 0.35%, respectively. Due to the simplification of FOMeT in solid phase and electrolyte phase diffusion, there is still a slight voltage and temperature error between FOMeT and P2D thermal model. Nevertheless, the error between FOMeT and P2D thermal model is smaller than that between FOM and P2D thermal model. FOMeT can effectively characterize the cell heat generation characteristics and thermal effect.

Table 3 shows the calculation time of FOM, FOMeT, and P2D thermal model. All simulation are run in Window 11 with Intel(R) Core(TM) i7-10700F CPU @ 2.90 GHz, 16.0GB RAM. Although the calculation speed of FOMeT is slower than that of FOM, it is much faster than the P2D thermal model. FOMeT has a fast running speed while ensuring high accuracy in voltage and temperature prediction, which provides the possibility for FOMeT application in BMS.

To verify the accuracy of FOMeT at different temperature and current rates, FOMeT, FOM, and P2D thermal model discharge from 4.2 V to 2.5 V at 0.5C, 1C, and 2C rates at 273.15 K, 298.15 K, and 318.15 K ambient temperature, respectively. The simulation results are shown in Fig. 6.

In Fig. 6(a), (c), (e), the voltage error between FOMeT and P2D thermal model increases with growing discharge rate. As the ambient temperature decreases, the solid and electrolyte phase diffusion slowing down leads to polarization increasing polarization in solid and electrolyte phase. Therefore, the cell reaches the cut-off voltage in advance. In Fig. 6(b), (d), (f), the larger the cell discharge rate is, the larger the cell temperature rises. As the ambient temperature decreases, the ohmic resistance, the heat generation rate, and the temperature rise rate of the cell increase at the same time. However, since the galvanostatic discharge time is shorter at low ambient temperature, the maximum temperature rises of the cell operating at low ambient temperature is lower than that operating at high temperature.

The P2D thermal model is taken as the criterion, the MAPE and RMSE of the FOM voltage relative to the P2D thermal model voltage are shown in Table 4. Compared with the P2D thermal model, the maximum voltage error of FOM occurs when the ambient temperature is 298.15 K and the discharge rate is 2C, and its MAPE and RMSE are 2.47% and 85.17 mV, respectively.

The P2D thermal model is taken as the criterion, the MAPE and RMSE of the voltage and temperature of FOMeT compared with P2D thermal model are shown in Table 5. The maximum voltage error of FOMeT occurs when the ambient temperature is 318.15 K and the discharge rate is 2C. Its MAPE and RMSE are 1.39% and 47.65 mV, respectively. The maximum temperature error of FOMeT occurs when the ambient temperature is 273.15 K and the discharge rate is 2C, and its MAPE and RMSE are 0.00468% and 0.0129 K, respectively.

The simulation results show that FOMeT has higher voltage prediction accuracy than the FOM model at various temperature and discharge rate. FOMeT can effectively reflect the heat dissipation of the cell and can precisely predict the temperature of the cell.

Table 3
Calculation time of FOM, FOMeT and P2D thermal model.

Battery model	Calculation Time
FOM	0.457s
FOMeT	6.868s
P2D thermal model	44 min10 s

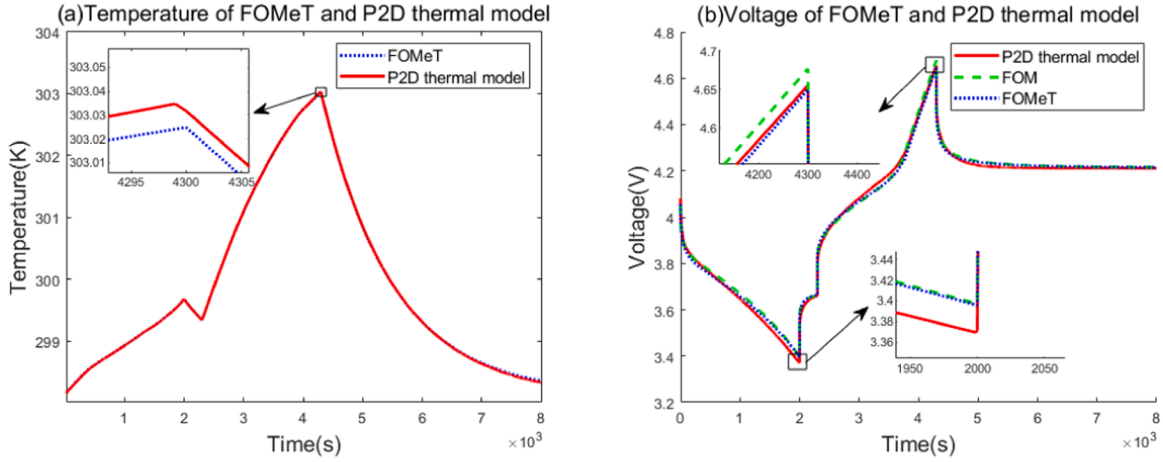

Fig. 5. Temperature and voltage comparison between FOMeT and P2D thermal model. (a) Temperature of FOMeT and P2D thermal model. (b) Voltage of FOMeT and P2D thermal model.

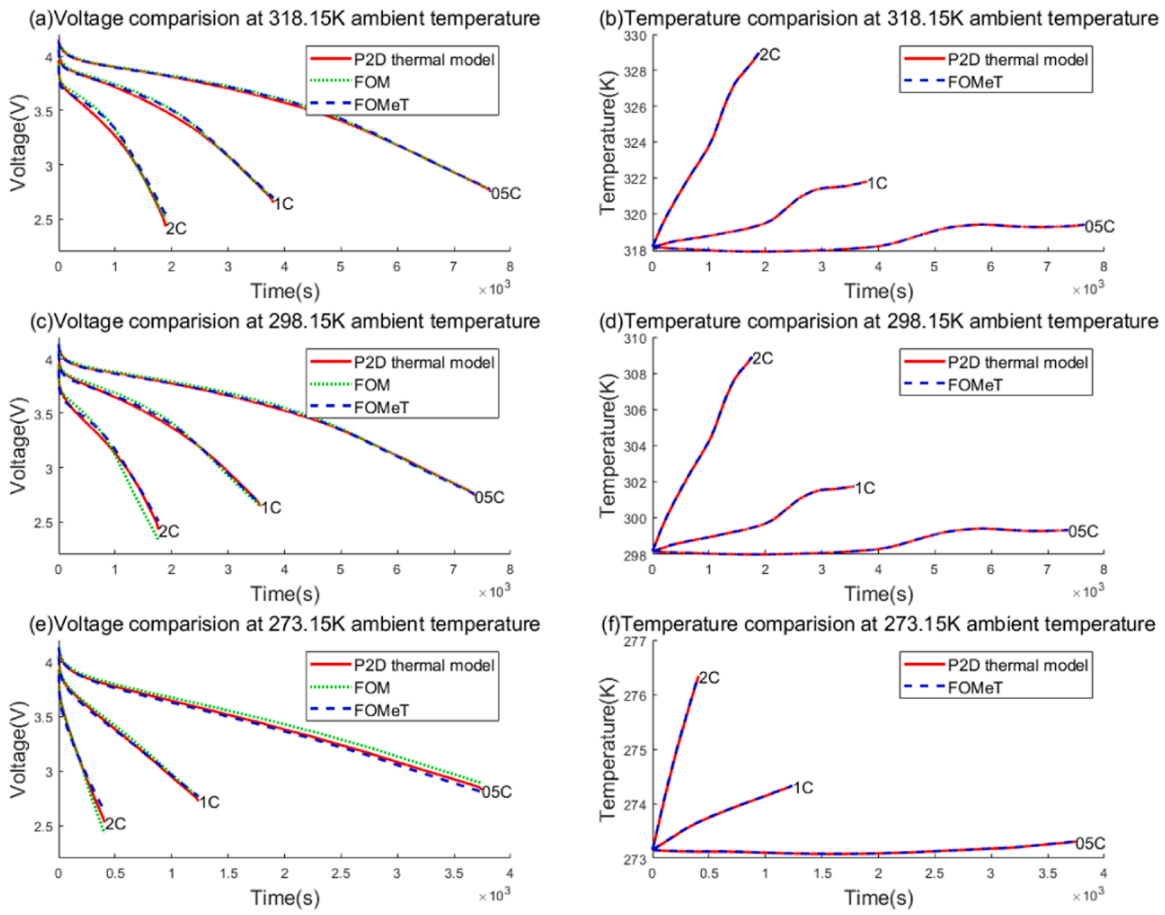

Fig. 6. Temperature and voltage comparison among FOM, FOMeT and P2D thermal model. (a), (c), (e) Cell voltage of FOMeT, FOM and P2D thermal model simulated at 0.5C, 1C, 2C discharging rates and 273.15 K, 298.15 K, 318.15 K ambient temperature, respectively. (b), (d), (f) Cell temperature of FOMeT and P2D thermal model simulated at 0.5C, 1C, 2C discharging rates and 273.15 K, 298.15 K, 318.15 K ambient temperature, respectively.

Table 4
Voltage errors between FOM and P2D thermal model.

Ambient temperature (*K*)	Discharge rate (C)	Voltage MAPE(%)	RMSE(mV)
318.15	0.5C	0.33%	14.84
	1C	0.66%	28.7
	2C	1.16%	47.68
298.15	0.5C	0.41%	17.12
	1C	0.92%	33.63
	2C	2.47%	85.17
273.15	0.5C	1.18%	40.91
	1C	0.75%	25.41
	2C	1.26%	49.94

Table 5
Voltage and temperature errors between FOMeT and P2D thermal model.

Ambient temperature (*K*)	Discharge rate (C)	Voltage MAPE (%)	RMSE (mV)	Temperature MAPE(%)	RMSE(K)
318.15	0.5C	0.28%	12.54	0.00090%	0.0039
	1C	0.59%	24.39	0.00190%	0.007
	2C	1.39%	47.65	0.00480%	0.0165
298.15	0.5C	0.20%	7.74	0.00087%	0.0035
	1C	0.41%	15.88	0.00187%	0.0063
	2C	0.89%	32.61	0.00500%	0.016
273.15	0.5C	0.61%	21.35	0.00058%	0.002145
	1C	0.41%	15.41	0.00159%	0.004585
	2C	1.30%	44.53	0.00468%	0.012938

4. Conclusion

This paper mainly focuses on the simplification of the electrochemical-thermal coupling model. A fractional-order model of lithium-ion battery considering polarization in electrolyte and thermal effect is proposed. The Padé approximation is applied to simplify the diffusion of lithium-ion in the solid phase, and the coefficients of the first-order Padé approximation are identified by PSO algorithm. The polynomial approximation is adopted to simplify the electrolyte diffusion of lithium-ion. Meanwhile, a particle thermal model is proposed to describe the heat exchange between the cell and the environment, and its equivalent heat dissipation coefficient is also identified. Then, the FOMeT is established by combining simplified electrochemical model and particle thermal model. The temperature dependent parameters of the simplified electrochemical model change with the cell temperature, and the cell temperature changes with heat generation of FOMeT. Compared with other electrochemical models, there are some conclusions of FOMeT.

Firstly, FOMeT is a simplified electrochemical-thermal coupling model with high computational efficiency. FOMeT simplifies solid-phase and electrolyte-phase lithium-ion diffusion equation, and heat exchange between the cell and the environment. The results show that FOMeT can greatly save computation time compared with P2D thermal coupling model.

Secondly, FOMeT is a physics-based lithium-ion battery model, which considers solid-phase diffusion polarization, electrolyte-phase diffusion polarization, electrochemical reaction polarization, and ohmic polarization. The simulation results show that FOMeT has higher

voltage prediction accuracy than FOM.

Finally, the simplified electrochemical model innovatively combines with the particle thermal model to capture thermal characteristic and lithium-ion dynamics of the cell. The results show that FOMeT has high voltage prediction accuracy and cell temperature prediction accuracy under the current rates from 0.5C to 2C and the temperature range from 273.15 K to 318.15 K. The MAPE and RMSE value of the terminal voltage of FOMeT relative to that of P2D thermal model are less than 1.39% and 47.65 mV, respectively. The maximum temperature error of FOMeT relative to that of P2D thermal model is less than 0.029 K.

CRediT authorship contribution statement

Guorong Zhu: Methodology, Investigation, Formal analysis. **Chun Kong:** Methodology, Investigation, Writing – original draft. **Jing V. Wang:** Conceptualization, Writing – review & editing. **Jianqiang Kang:** Formal analysis, Supervision, Writing – review & editing. **Geng Yang:** Conceptualization, Writing – review & editing. **Qian Wang:** Formal analysis, Writing – review & editing.

Declaration of Competing Interest

The authors declare that they have no known competing financial interests or personal relationships that could have appeared to influence the work reported in this paper.

Data availability

No data was used for the research described in the article.

Acknowledgement

This work was supported by the National Natural Science Foundation of China under Grants No. 52277224, No. 51977163, and Science and Technology on Ship Integrated Technology Laboratory under Grants No.614221720200306.

References

[1] Y. Chen, Y. Kang, Y. Zhao, et al., A review of lithium-ion battery safety concerns: the issues, strategies, and testing standards[J], J. Energy Chem. 59 (2021) 83–99, https://doi.org/10.1016/j.jechem.2020.10.017.
[2] Z. Li, J. Huang, B.Y. Liaw, et al., On state-of-charge determination for lithium-ion batteries[J], J. Power Sources 348 (2017) 281–301, https://doi.org/10.1016/j.jpowsour.2017.03.001.
[3] X. Sun, J. Ji, B. Ren, et al., Adaptive forgetting factor recursive least square algorithm for online identification of equivalent circuit model parameters of a lithium-ion battery: 12[J], Energies 12 (12) (2019) 2242, https://doi.org/10.3390/en12122242.
[4] X. Gao, X. Li, F. Wang, et al., A simplified electrochemical model of lithium-ion battery considering liquid overpotential[C]//, in: IEEE International Conference on Sensing, Diagnostics, Prognostics, and Control (SDPC), 2021, https://doi.org/10.1109/SDPC52933.2021.9563403.
[5] M. Doyle, T.F. Fuller, J Newman, Modeling of galvanostatic charge and discharge of the lithium/polymer/insertion cell[J], J. Electrochem. Soc. 140 (6) (1993) 1526, https://doi.org/10.1149/1.2221597.
[6] J. Li, L. Zou, F. Tian, et al., Parameter identification of lithium-ion batteries model to predict discharge behaviors using heuristic algorithm[J], J. Electrochem. Soc. 163 (8) (2016) A1646–A1652, https://doi.org/10.1149/2.0861608jes.
[7] Z.-Yu Liu, K.U.N. Yang, ZI-Hong Wei, et al., Electrochemical model of lithium ion battery with simplified liquid phase diffusion equation[J], Acta Phys. Sin. 68 (9) (2019), 098801, https://doi.org/10.7498/aps.68.20190159 (8 pp.).
[8] S. Han, Y. Tang, R.S Khaleghi, A numerically efficient method of solving the full-order pseudo-2-dimensional (p2d) li-ion cell model[J], J. Power Sources 490 (2021), 229571, https://doi.org/10.1016/j.jpowsour.2021.229571.
[9] S. Santhanagopalan, Q. Guo, P. Ramadass, et al., Review of models for predicting the cycling performance of lithium ion batteries[J], J. Power Sources 156 (2) (2006) 620–628, https://doi.org/10.1016/j.jpowsour.2005.05.070.
[10] N. Lotfi, J. Li, R.G. Landers, et al., Li-ion battery state of health estimation based on an improved single particle model[C]//, in: 2017 American Control Conference (ACC), 24-26 May 2017. Piscataway, NJ, USA, IEEE, 2017, pp. 86–91, https://doi.org/10.23919/ACC.2017.7962935.
[11] D. Guo, G. Yang, X. Feng, et al., Physics-based fractional-order model with simplified solid phase diffusion of lithium-ion battery[J], J. Energy Storage 30 (2020), 101404, https://doi.org/10.1016/j.est.2020.101404.
[12] J. Tian, R. Xiong, W. Shen, et al., Online simultaneous identification of parameters and order of a fractional order battery model[J], J. Clean. Prod. 247 (2020), 119147, https://doi.org/10.1016/j.jclepro.2019.119147.
[13] P. Hashemzadeh, M. Désilets, M. Lacroix, et al., Investigation of the p2d and of the modified single-particle models for predicting the nonlinear behavior of li-ion batteries[J], J. Energy Storage 52 (2022), 104909, https://doi.org/10.1016/j.est.2022.104909.
[14] X. Han, M. Ouyang, L. Lu, et al., Simplification of physics-based electrochemical model for lithium ion battery on electric vehicle. part i: diffusion simplification and single particle model[J], J. Power Sources 278 (2015) 802–813, https://doi.org/10.1016/j.jpowsour.2014.12.101.
[15] S.J. Moura, F.B. Argomedo, R. Klein, et al., Battery state estimation for a single particle model with electrolyte dynamics[J], IEEE Trans. Control Syst. Technol. 25 (2) (2017) 453–468, https://doi.org/10.1109/TCST.2016.2571663.
[16] M. Guo, G. Sikha, R.E White, Single-particle model for a lithium-ion cell: thermal behavior[J], J. Electrochem. Soc. 158 (2) (2010) A122, https://doi.org/10.1149/1.3521314.
[17] C. Li, N. Cui, C. Wang, et al., Simplified electrochemical lithium-ion battery model with variable solid-phase diffusion and parameter identification over wide temperature range[J], J. Power Sources 497 (2021), 229900, https://doi.org/10.1016/j.jpowsour.2021.229900.
[18] Y. Ma, X. Li, G. Li, et al., SOC oriented electrochemical-thermal coupled modeling for lithium-ion battery[J], IEEE Access 7 (2019) 156136–156149, https://doi.org/10.1109/ACCESS.2019.2949357.
[19] L. Wu, K. Liu, H Pang, Evaluation and observability analysis of an improved reduced-order electrochemical model for lithium-ion battery[J], Electrochim. Acta 368 (2021), 137604, https://doi.org/10.1016/j.electacta.2020.137604.
[20] Q. Zhang, Q. Guo, R.E White, Semi-empirical modeling of charge and discharge profiles for a licoo2 electrode[J], J. Power Sources 165 (1) (2007) 427–435, https://doi.org/10.1016/j.jpowsour.2006.12.025.
[21] S. Yuan, L. Jiang, C. Yin, et al., A transfer function type of simplified electrochemical model with modified boundary conditions and padé approximation for li-ion battery: part 1. lithium concentration estimation[J], J. Power Sources 352 (2017) 245–257, https://doi.org/10.1016/j.jpowsour.2017.03.060.
[22] S. Yuan, L. Jiang, C. Yin, et al., A transfer function type of simplified electrochemical model with modified boundary conditions and padé approximation for li-ion battery: part 2. modeling and parameter estimation[J], J. Power Sources 352 (2017) 258–271, https://doi.org/10.1016/j.jpowsour.2017.03.061.
[23] W. Luo, C. Lyu, L. Wang, et al., An approximate solution for electrolyte concentration distribution in physics-based lithium-ion cell models[J], Microelectron. Reliab. 53 (6) (2013) 797–804, https://doi.org/10.1016/j.microrel.2012.11.002.
[24] C. Li, N. Cui, C. Wang, et al., Reduced-order electrochemical model for lithium-ion battery with domain decomposition and polynomial approximation methods[J], Energy 221 (2021), 119662, https://doi.org/10.1016/j.energy.2020.119662.
[25] W. Luo, C. Lyu, L. Wang, et al., A new extension of physics-based single particle model for higher charge–discharge rates[J], J. Power Sources 241 (2013) 295–310, https://doi.org/10.1016/j.jpowsour.2013.04.129.
[26] D. Bernardi, E. Pawlikowski, J Newman, A general energy balance for battery systems[J], J. Electrochem. Soc. 132 (1) (1985) 5, https://doi.org/10.1149/1.2113792.
[27] D. Li, L. Yang, C Li, Control-oriented thermal-electrochemical modeling and validation of large size prismatic lithium battery for commercial applications[J], Energy 214 (2021), 119057, https://doi.org/10.1016/j.energy.2020.119057.
[28] D. Wang, H. Huang, Z. Tang, et al., A lithium-ion battery electrochemical–thermal model for a wide temperature range applications[J], Electrochim. Acta 362 (2020), 137118, https://doi.org/10.1016/j.electacta.2020.137118.
[29] V. Srinivasan, C.Y Wang, Analysis of electrochemical and thermal behavior of li-ion cells[J], J. Electrochem. Soc. 150 (1) (2002) A98, https://doi.org/10.1149/1.1526512.
[30] K. Kumaresan, G. Sikha, R.E White, Thermal model for a li-ion cell[J], J. Electrochem. Soc. 155 (2) (2007) A164, https://doi.org/10.1149/1.2817888.
[31] H. Yuan, S. Zhu, S. Akehurst, et al., A novel numerical implementation of electrochemical-thermal battery model for electrified powertrains with conserved spherical diffusion and high efficiency[J], Int. J. Heat Mass Transf. 178 (2021), 121614, https://doi.org/10.1016/j.ijheatmasstransfer.2021.121614.
[32] W-J Shen, H-X. Li, Multi-scale parameter identification of lithium-ion battery electric models using a pso-lm algorithm: 4[J], Energies 10 (4) (2017) 432, https://doi.org/10.3390/en10040432.
[33] M. Doyle, J. Newman, A.S. Gozdz, et al., Comparison of modeling predictions with experimental data from plastic lithium ion cells[J], J. Electrochem. Soc. 143 (6) (1996) 1890, https://doi.org/10.1149/1.1836921.